Journal of Hazardous Materials 178 (2010) 440–449

Contents lists available at ScienceDirect

Journal of Hazardous Materials

journal homepage: www.elsevier.com/locate/jhazmat

Synthesis and characterization of $La_2O_3/TiO_{2-x}F_x$ and the visible light photocatalytic oxidation of 4-chlorophenol

Guangxiu Cao[a,b], Yaogang Li[a], Qinghong Zhang[c,*], Hongzhi Wang[a,*]

[a] State Key Laboratory for Modification of Chemical Fibers and Polymer Materials, Donghua University, Shanghai 201620, PR China
[b] Department of Chemistry, Shangqiu Normal University, Shangqiu 476000, PR China
[c] Engineering Research Center of Advanced Glasses Manufacturing Technology, MOE, Donghua University, Shanghai 201620, PR China

ARTICLE INFO

Article history:
Received 19 July 2009
Received in revised form
15 December 2009
Accepted 19 January 2010
Available online 28 January 2010

Keywords:
Visible light
Photocatalytic oxidation
TiO_2
4-Chlorophenol

ABSTRACT

In this work, we investigated the synergetic effect of La and F on the visible light photocatalytic activity of TiO_2 catalysts. $La_2O_3/TiO_{2-x}F_x$ photocatalysts were prepared by a simple sol-gel process using tetrabutyl titanate (TBT), $La(NO_3)_3$ and NH_4F as precursors. XPS results revealed that La_2O_3 accumulated on the surface of TiO_2, which enhanced the surface area of TiO_2 and inhibited the recombination of electron–hole pairs. It also showed that two kinds of fluorine species were formed and these increased the acid active sites and enhanced the oxidation potential of the photogenerated holes in the valance band. UV–vis diffuse reflection spectra of $La_2O_3/TiO_{2-x}F_x$ showed that intraband gap states were present and these are probably responsible for its absorption of visible light while the intrinsic absorption band was shifted slightly to a longer wavelength. At molar ratios of La and F to Ti of 1.5:100 and 5:100 and after calcination at 500 °C, the degradation rate of 4-chlorophenol (4-CP) over the sample was about 1.2–3.0 times higher than that of the other doped samples and undoped TiO_2. The total organic carbon (TOC) removal rates of 4-CP showed that 4-CP was mineralized efficiently in the presence of the sample under visible light illumination.

© 2010 Elsevier B.V. All rights reserved.

1. Introduction

In recent years, photocatalysts have attracted considerable attention as they can be used to treat organic pollutants, purify air and produce hydrogen by photocatalytically splitting water [1–10]. Among the oxide semiconductor photocatalysts, titania is currently a promising photocatalyst because of its low cost, non-toxicity, chemical stability and the strong oxidizing power of its photogenerated holes. However, its practical application as a photocatalyst has been limited because of its large energy bandgap (~3.2 eV) which requires UV light with a wavelength of less than 385 nm. UV light only makes up about 3–5% of the solar light spectrum and to better utilize solar light and indoor illumination extending the spectral response of these photocatalysts into the visible light region and enhancing their photocatalytic activities is a formidable challenge.

Doping with foreign elements such as metals [11–15] and non-metals improves the energy band structure of TiO_2 by shifting its optical absorption into the visible light region. Since nitrogen-doped TiO_2 was first reported by Asahi et al. [3], doping with non-metals such as N [3,16–19], C [20], B [21–24], S [25], I [26] and F [27,28], has received a great deal of attention. Although these doped TiO_2 photocatalysts do have a response in the visible light region, there is no guarantee that they will enhance the photocatalytic activity [23]. For example, using boron as a dopant resulted in an extended optical absorption and enhanced photocatalytic activity in one study [23] while in other studies [21,22] inconsistent results were reported.

To further extend the optical absorption and enhance the visible light photocatalytic activity of TiO_2, many researchers are studying the synergetic effect of non-metal co-doping such as N–C co-doping [29,30], S–C co-doping [31] and B–N co-doping [23,32]. Non-metal co-doping has been reported to improve the photocatalytic characteristics of TiO_2 but some negative effects in these systems are still under investigation. First, non-metal co-doping atoms can result in more oxygen vacancies, which can form recombination centers for electron and hole pairs. Second, these doping elements do not effectively enhance the surface area of co-doped TiO_2 during the heat treatment step, which decreases the amount of organic compound adsorption on the surface of TiO_2. Third, the orbital energies of B_{2p}, C_{2p}, N_{2p} and S_{3p} are higher than that of O_{2p} according to hybrid orbital theory. Therefore, the valence band energy for TiO_2 increases because the valence band is made up of O_{2p} and B_{2p} or C_{2p}, N_{2p} and S_{3p}. The oxidation potential of the photogenerated holes in doped TiO_2 is, therefore, lower and this results in lower photocatalytic activity. Recently, lanthanum and iodine co-doped

* Corresponding author.
E-mail addresses: zhangqh@dhu.edu.cn (Q. Zhang), wanghz@dhu.edu.cn (H. Wang).

0304-3894/$ – see front matter © 2010 Elsevier B.V. All rights reserved.
doi:10.1016/j.jhazmat.2010.01.101

titania has been synthesized by He et al. Their results showed that lanthanum can act as a barrier and thus facilitate charge carrier separation while the dopant lanthanum can create a Ti^{3+} state, which retards the recombination of electron–hole pairs and extends the absorption into the visible light region. Moreover, the dopant iodine enters the lattice of TiO_2 and then I^{5+} replaces Ti^{4+} to maintain the charge balance [26]. Three positive roles for the fluorine dopant during photocatalysis are considered. First, physically adsorbed fluorine ions can increase the number of active sites on the surface of TiO_2 [19]. Second, the Ti^{3+} state and oxygen vacancies are created by fluorine doping below the conduction band [33]. Therefore, the electrons in the valence band will transfer to the 3d states of Ti^{3+} and/or oxygen vacancies under visible light irradiation. The photogenerated electrons will then combine with the O_2 adsorbed on the surface of TiO_2 to form superoxide anions [34]. Third, doped fluorine can result in a localized level with high density below the valence band of TiO_2, which is beneficial in enhancing the oxidation potential of the valance band holes and capturing surface hydroxyls to produce $^{\bullet}OH$ [18,35].

In this paper, we demonstrate a synergetic effect of La and F on the visible light photocatalytic activity of TiO_2. $La_2O_3/TiO_{2-x}F_x$ shows a spectral response into the visible light region and also exhibits significantly enhanced photocatalytic activity. After the photocatalytic degradation of 4-chlorophenol, a TOC analysis verified that the visible light photocatalytic activity of TiO_2 was enhanced by the synergetic effect of La and F. Therefore, it has potential to be used in a practical application.

2. Experimental

2.1. Synthesis

All chemicals used in this study were of analytical grade and millipore water was used in all experiments. Typically, tetrabutyl titanate, NH_4F and $La(NO_3)_3$ were used as sources of TiO_2, fluorine and lanthanum, respectively. 0.01–0.02 mol NH_4F was dissolved in 100 mL millipore water, 0.2 mol tetrabutyl titanate and 0.002–0.004 mol $La(NO_3)_3$ were dissolved in 100 mL dry alcohol and then the mixed solution of tetrabutyl titanate and $La(NO_3)_3$ was added dropwise to 100 mL of the NH_4F solution under vigorous stirring at room temperature using different atomic ratios of F and La to Ti. The mixed solution was stirred in a closed beaker at room temperature for 12 h to further hydrolyze tetrabutyl titanate and monodispersed TiO_2 particles were obtained. The sol solution was dried at 100 °C for 10 h in air to remove water and alcohol and a xerogel was obtained. After calcination at high temperature in air for 2 h, a white powder was obtained. The lanthanum and fluorine co-doped TiO_2 nanoparticles were denoted L_xF_yT-t, where x, y and t represent the atomic ratios of La and F to Ti and the calcination temperature in degrees Celsius, respectively. For comparison, pure TiO_2 was also prepared using the same procedure without NH_4F and $La(NO_3)_3$.

2.2. Characterization

The powder phase composition was identified by X-ray diffraction (XRD) equipment using Cu Kα (λ = 1.5406 Å) radiation. UV–vis diffuse reflection spectra were recorded on a PE Lambda 950 instrument in the form of a dry-pressed disk at room temperature. $BaSO_4$ was used as a reference from 200 to 800 nm. Particle morphology was observed with a JEM-100CX II transmission electron microscope (TEM). Specific surface areas were determined by nitrogen adsorption desorption isotherm measurements at 77 K on an Autosorb-1 nitrogen adsorption apparatus (Quantachrome Instruments, USA).

X-ray photoelectron spectroscopy (XPS) was performed using a Kratos Axis Ultra system with monochromatic Al Kα X rays (1486.6 eV) operated at 75 W and 15 kV with a background pressure of approximately 5.0×10^{-9} Torr. A survey spot size and 40 eV pass energy were used for the analysis. Photoelectrons emitted perpendicular to the sample surface were collected. A charge neutralizer was used and all the binding energies were calibrated with respect to the adventitious contamination hydrocarbon C_{1s} peak at 284.8 eV.

2.3. Photocatalytic activity measurements

The photocatalytic oxidation of 4-CP was used as a model reaction to evaluate the photocatalytic activity of the resultant bare TiO_2 and doped TiO_2 powders. A top-irradiation reactor was used as the photoreactor. Irradiation was performed with a 500 W xenon lamp and a ZJB 420 filter glass was used to cut off light of wavelength <420 nm. In a typical reaction, 0.2 g of photocatalyst was added to a 450 mL Pyrex photoreactor containing 150 mL of 2.5×10^{-4} M 4-CP solution. The aqueous suspension was stirred for 30 min to establish an adsorption–desorption equilibrium for 4-CP in the dark and then it was irradiated under visible light. The light intensity at 420 nm near the surface of the 4-CP solution was identified as 30 mW/cm^2 (Newport Power Meter Model 1918-C). The aqueous suspension was periodically taken from the reactor, centrifuged and the absorbance of the clear solution was measured on a PerkinElmer Lambda-35 spectrophotometer at 224 nm. The absorbance was converted to 4-CP concentration using a standard curve that showed a linear relationship between the concentration and the absorbance at this wavelength.

In order to investigate the long-term photocatalytic activity, $L_{1.5}F_5T$-500 was used to degrade 4-CP solutions four times. After the first run (visible light irradiation for 4 h) the solution was centrifuged and the photocatalyst was washed three times with Millipore water and dried at 100 °C for 6 h. The recovered photocatalyst was subsequently used to degrade a fresh 4-CP solution under the same irradiation conditions for 4 h. Then 3-cycle and 4-cycle were also carried out in the same process.

The degradation rates and the total organic carbon removal rates of 4-CP was calculated using formula (1) and formula (2):

$$\eta\ (\%) = \frac{C_0 - C}{C_0} \times 100 \quad (1)$$

$$\phi(\%) = \frac{m_0 - m}{m_0} \times 100 \quad (2)$$

where C_0 and C are the concentrations of the primal and remaining 4-CP, m_0 and m are the primal and remaining total organic carbon content.

3. Results and discussion

3.1. Crystal structure

Fig. 1A and B shows the XRD patterns of some samples. Clearly, anatase was the main crystal phase of the TiO_2 and traces of brookite as well as rutile are present. Additionally, the intensity of the rutile (except in $L_{1.5}F_0T$-600) and brookite peaks decreased for L_xF_yT-600 as the fluorine and lanthanum content increased indicating that lanthanum and fluorine can suppress the anatase to rutile transformation. No La_2O_3 was observed on the surface of the crystallites probably because small amounts of La_2O_3 were present. This was similar to the results reported by He et al. [26]. We also found that the anatase peaks of these samples became wider as the lanthanum content increased, which means that the size of the TiO_2 nanoparticles decreased with increasing of lanthanum content. The decrease in crystallite size can be attributed to segregation

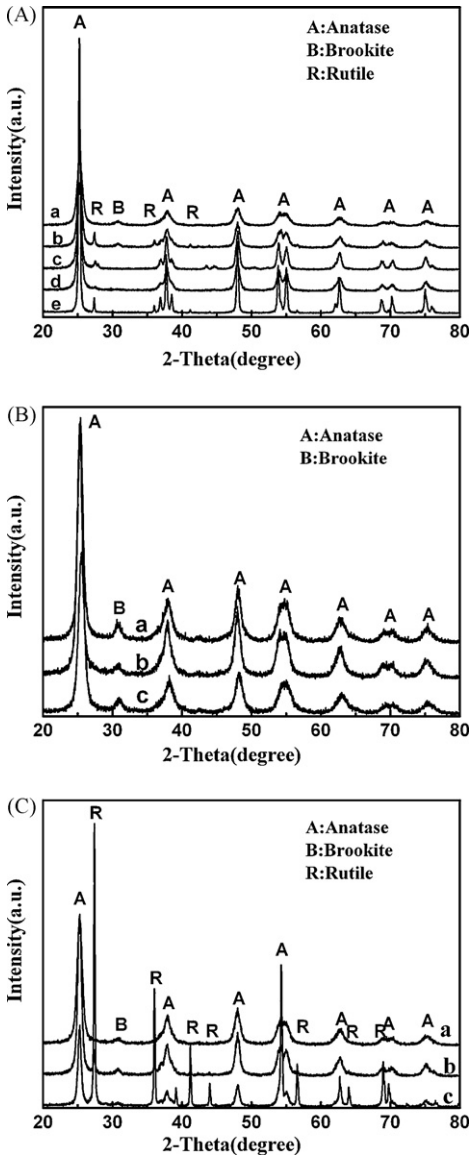

Fig. 1. The X-ray diffraction (XRD) patterns of (A): (a) $L_{1.5}F_0T$-600, (b) $L_{1.5}F_5T$-600, (c) $L_{1.5}F_{10}T$-600, (d) $L_{1.5}F_{20}T$-600 and (e) pure TiO_2; (B): (a) L_1F_5T-500, (b) $L_{1.5}F_5T$-500 and (c) L_2F_5T-500; (C): (a) $L_{1.5}F_5T$-500, (b) $L_{1.5}F_5T$-600 and (c) $L_{1.5}F_5T$-700.

after the formation of La_2O_3 at the grain boundary or the presence of the Ti–O–La bond, which inhibits the growth of crystal grains by restricting the coalescence of some smaller neighboring grains [36–38]. According to a line width analysis of the anatase (1 0 1) diffraction peak and based on the Scherrer's formula, the average crystallite sizes of some samples were estimated and the values are shown in Table 1 along with other physical characteristics. It can be seen from Table 1 that the cell parameters "*c*" of the doping samples decreased after modification with lanthanum and fluorine. This can be explained as follows: For the La-doped TiO_2 system, the ionic radius of La^{3+} (0.1016 nm) is much larger than that of Ti^{4+} (0.068 nm); Ti^{4+} can enter the lattice of La_2O_3 during heat treatment, which results in a TiO_2 lattice defect. Moreover, the doped fluorine ion in the O^{2-} sites of the TiO_2 lattice causes a reduction of Ti^{4+} to Ti^{3+}, which results in a TiO_2 lattice change. Therefore, the cell parameter "*c*" of the doping samples decreases after modification with lanthanum and fluorine. BET surface areas of the samples are also shown in Table 1. It is clear that the BET surface areas of the samples increase as the amount of lanthanum increases. This further confirms that lanthanum can efficiently inhibit the crystal growth of TiO_2. These results are consistent with the report by Reddy and Ganesh [39]. The BET surface areas of doped TiO_2 are less affected by fluorine doping because the oxygen ion radius (0.132 nm) and the fluorine ion radius (0.133 nm) are almost equal.

Fig. 1C shows the effect of calcination temperature on the phase structure of $L_{1.5}F_5T$-*t*. It can be seen that as the calcination temperature is increased from 500 to 700 °C, the width of the diffraction peaks of anatase become narrower suggesting that the crystallite sizes of $L_{1.5}F_5T$-*t* gradually become larger. Moreover, it is clear that the rutile phase peaks of the $L_{1.5}F_5T$-*t* samples increased as the calcination temperature increased from 500 to 700 °C, which means that lanthanum and fluorine ions cannot suppress the anatase to rutile transformation when the calcination temperature is increased. This can be attributed to three factors: First, the metal cation (Ti^{4+}) is hydrolyzed to form $Ti(OH)_4$ and then $Ti(OH)_{4-x}F_x$ because of the strong electronegativity of fluorine. As the temperature is increased, $Ti(OH)_{4-x}F_x$ decomposes and this is a fast reaction. This fast reaction rate promotes the formation of anatase rather than the thermodynamically favorable rutile. Upon further heating, the fluorine atoms are preferentially eliminated, causing faster atomic/ionic diffusion. These faster diffusion conditions are favorable for the formation of a denser rutile structure [40]. Second, the phase transformation involves a rearrangement of the (TiO_6) octahedron [41] and the surface La_2O_3 species may prevent the TiO_2 nanoparticles from agglomerating and rearranging during calcination which retards the anatase to rutile transformation. Third, the pore volume for $L_{1.5}F_5T$-500 and undoped TiO_2 was 0.1625 and 0.1026 cm^3/g, respectively. It is clear that La_2O_3 accumulated on the surface of TiO_2 nanoparticles could inhibit the agglomeration of TiO_2 particles, which can produce more disordered pores, the porous structure formed might inhibit the migration and arrangement of the Ti and O atoms during the formation of rutile during calcination [24].

3.2. TEM images

Fig. 2 shows TEM images of the $L_{1.5}F_5T$-*t* sample calcined at different temperatures and also the L_2F_5T-500 samples. Clearly, the nanocrystal size of $L_{1.5}F_5T$-*t* gradually increases as the calcination temperature is increased from 500 to 700 °C. At 700 °C, some of the

Table 1
Crystallite size, lattice parameters and BET surface areas of the undoped and doped TiO_2.

Sample	Crystallite size (nm) (anatase)	Lattice parameter (*a*, Å) (anatase)	Lattice parameter (*c*, Å) (anatase)	S_{BET} (m^2/g)
TiO_2-600	32.7	3.7881	9.5247	19
TiO_2-500	25.4	3.7880	9.5238	25
L_1F_5T-500	12.4	3.7875	9.4986	44
$L_{1.5}F_5T$-500	11.3	3.7894	9.4936	69
L_2F_5T-500	11.2	3.7875	9.5152	74
L_1F_5T-600	14.2	3.7849	9.5075	33
$L_{1.5}F_5T$-600	13.8	3.7851	9.4862	40
$L_{1.5}F_5T$-700	16.5	3.7867	9.5196	16
$L_{1.5}F_{10}T$-500	11.1	3.7894	9.4936	70

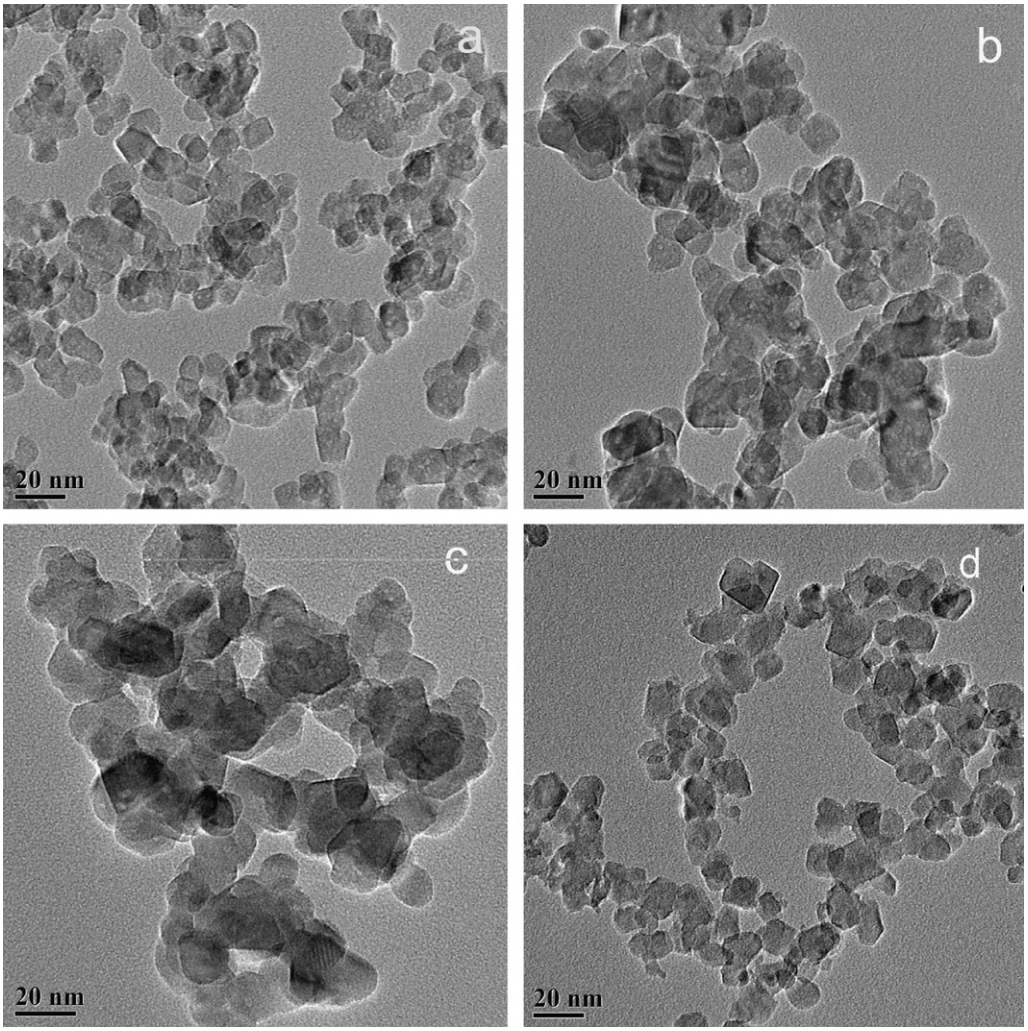

Fig. 2. TEM images of lanthanum and fluorine co-doped TiO_2 samples with $x = 1.5$, $y = 5$ and calcined at (a) 500 °C, (b) 600 °C, (c) 700 °C and (d) L_2F_5T-500.

particles agglomerate resulting in the BET surface areas decreasing to 16 m^2/g. Compared with the $L_{1.5}F_5T$-500 sample, the L_2F_5T-500 sample has a smaller crystallite size, implying that lanthanum dopants could inhibit the growth of crystal grains. Moreover, no La_2O_3 was observed on the crystallite surfaces probably because of the small amount of La_2O_3 present.

3.3. Nitrogen adsorption–desorption

Fig. 3 shows nitrogen adsorption–desorption isotherms and BJH pore size distribution curves for $L_{1.5}F_5T$-500, $L_{1.5}F_5T$-600 and $L_{1.5}F_5T$-700. The adsorption isotherms (Fig. 3A) are typical type IV with a hysteresis loop according to the IUPAC classification, indicating that the powders contain disordered mesopores [42]. The formation of the mesopores can be explained as follows: First, monodispersed amorphous titanium oxide sol particles are formed by the hydrolysis of tetrabutyl titanate and subsequent condensation under heat treatment. The monodispersed xerogel particles then crystallize and aggregated during heat treatment to form mesoporous crystalline TiO_2 [43–45]. The pore size distribution curves (Fig. 3B) were calculated from the desorption branch of a nitrogen isotherm by the BJH method using the Halsey equation and showed that all three samples had a narrow pore size distribution with a maximum around 2.3, 3.7 and 5.1 nm, respectively [27]. The BJH desorption cumulative pore volume of pores below 13 nm and the BET specific surface areas were 0.1625, 0.1365 and 0.1008 cm^3/g as well as 69, 40 and 16 m^2/g for $L_{1.5}F_5T$-500, $L_{1.5}F_5T$-600 and $L_{1.5}F_5T$-700, respectively.

3.4. XPS studies

Fig. 4A shows high-resolution XPS spectra of the F_{1s} region of $L_{1.5}F_5T$-500, $L_{1.5}F_5T$-600 and $L_{1.5}F_5T$-700. The XPS spectra of the F_{1s} region of the samples showed two separate peaks. The strong peak of F_{1s} is located at 684.5 eV and is assigned to fluorine ions that are physically adsorbed onto the surface of TiO_2 [28]. Physically adsorbed fluorine ions can enhance photocatalytic activity because they increase the number of active site on the surface of TiO_2 [19]. The weak peak of F_{1s} is located at 688.4 eV and is assigned to fluorine ions that are within the crystal lattice of TiO_2. The oxygen positions are thus occupied by fluorine, i.e., O–Ti–F bonds are formed. Fluorine doped TiO_2 can be represented as $TiO_{2-x}F_x$. A charge imbalance is created in the TiO_2 lattice so it needs one extra electron for charge compensation. This electron localizes on a lattice cation causing it to reduce from Ti^{4+} to Ti^{3+} according to polaron theory [46,47] and this is also indicated by Ti_{2p} analysis (see below). Doping with fluorine can result in a high density localized level and it is present below the valence band of TiO_2, which mainly consists of the F_{2p} state [18,35]. Therefore, holes in the valance band are trapped in these localized levels and are less mobile, which is beneficial in increasing the oxidation potential of the valance band holes and capturing surface hydroxyls to produce •OH (Scheme 1). •OH is

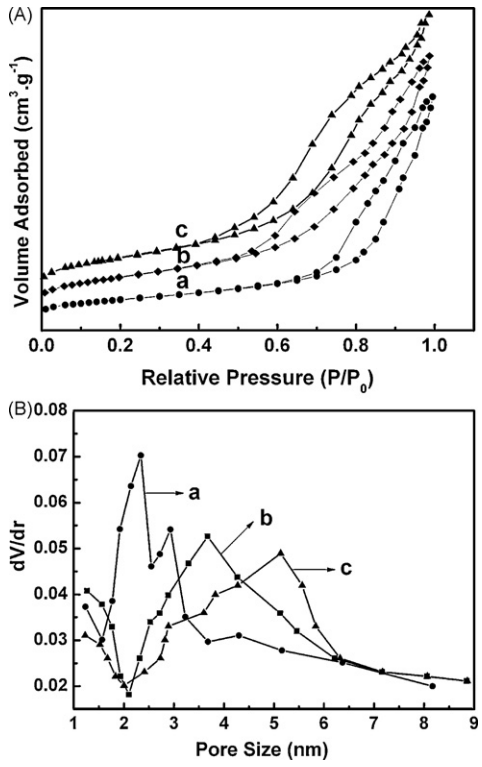

Fig. 3. Nitrogen adsorption–desorption isotherm (A) and pore size distribution (B) of (a) $L_{1.5}F_5T$-500, (b) $L_{1.5}F_5T$-600 and (c) $L_{1.5}F_5T$-700.

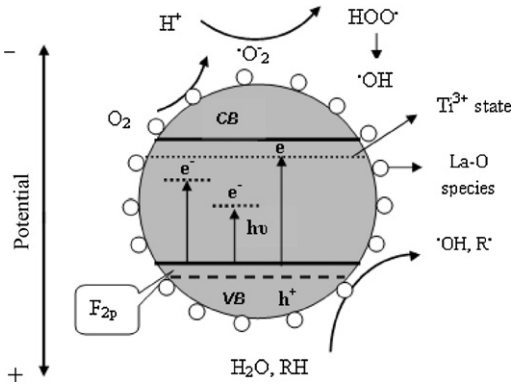

Scheme 1. Illustration of the photocatalytic mechanism under visible light irradiation.

a powerful oxidant for the degradation of 4-CP. As shown in Fig. 4B, the O_{1s} spectra of $L_{1.5}F_5T$-500, $L_{1.5}F_5T$-600 and $L_{1.5}F_5T$-700 mainly consist of three peaks at 530.2, 532.2 and 533.1 eV corresponding to Ti–O, the hydroxyl group and La–O, respectively [24].

Two characteristic doublet peaks of La_{3d} are present in Fig. 4C and these correspond to binding energies of 835.3 eV and 852.2 eV for the $La_{3d5/2}$ and $La_{3d3/2}$ levels. Compared with the standard spectra of lanthanum oxide, it is clear that the lanthanum bonded to oxygen was located at the sample surface at every calcination temperature and thus the photocatalyst can be represented by $La_2O_3/TiO_{2-x}F_x$. We also found that the intensity of the La_{3d} peaks gradually increased as the calcination temperature increased from 500 to 700 °C. This implies that a higher calcination temperature results in higher amounts of La_2O_3. The formation of La_2O_3 results in an efficient separation of the TiO_2 surface charge indicating that

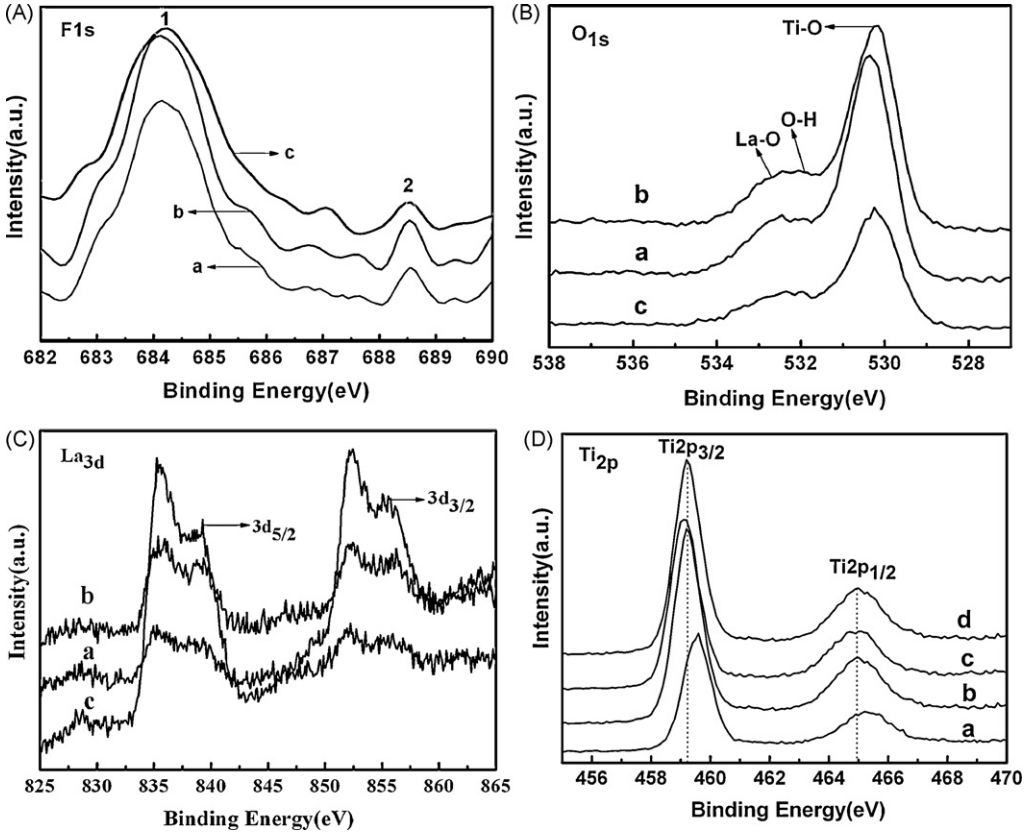

Fig. 4. The high-resolution XPS spectra (A) F_{1s} region of (a) $L_{1.5}F_5T$-500, (b) $L_{1.5}F_5T$-600 and (c) $L_{1.5}F_5T$-700; (B) O_{1s} region of (a) $L_{1.5}F_5T$-500, (b) $L_{1.5}F_5T$-600 and (c) $L_{1.5}F_5T$-700; (C) La_{3d} region of (a) $L_{1.5}F_5T$-500, (b) $L_{1.5}F_5T$-600 and (c) $L_{1.5}F_5T$-700; (D) Ti_{2p} region of (a) undoped TiO_2, (b) $L_{1.5}F_5T$-500, (c) $L_{1.5}F_5T$-600 and (d) $L_{1.5}F_5T$-700.

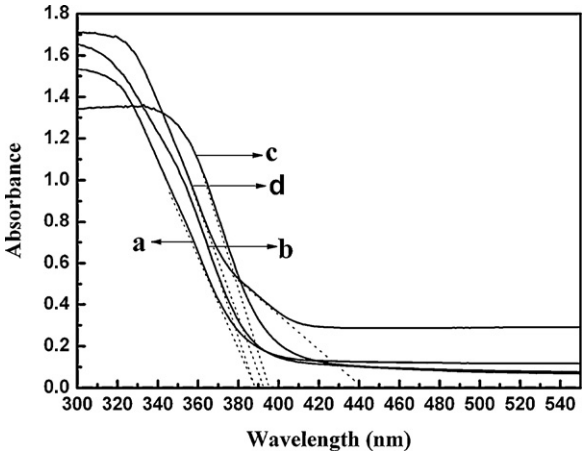

Fig. 5. The UV–vis diffuse reflection spectra of (a) undoped TiO_2, (b) L_0F_5T-500, (c) $L_{1.5}F_0T$-500 and (d) $L_{1.5}F_5T$-500.

it can inhibit the recombination of photogenerated electron–hole pairs and thus prolong the lifetime of electron–hole pairs [26]. Moreover, for the La-doped TiO_2 system, the ionic radius of La^{3+} (0.1016 nm) is much larger than that of Ti^{4+} (0.068 nm) indicating that the bulky lanthanum ions cannot substitute Ti^{4+} to form stable solid solutions. Therefore, Ti^{4+} can enter the lattice of lanthanum oxide during heat treatment, which creates a charge imbalance. The charge imbalance must be satiated and Ti^{4+} is thus reduced to Ti^{3+}, which is also indicated by Ti_{2p} analysis (see below).

As shown in Fig. 4D, the Ti_{2p} region of the undoped TiO_2, $L_{1.5}F_5T$-500, $L_{1.5}F_5T$-600 and $L_{1.5}F_5T$-700 show two peaks located at about 459 and 464.8 eV, which are assigned to $Ti_{2p_{3/2}}$ and $Ti_{2p_{1/2}}$, respectively. The typical binding energy of the $Ti_{2p_{3/2}}$ peak in TiO_2 crystals is 458.5–459.7 eV. Compared with the binding energy of $Ti_{2p_{3/2}}$ for the undoped sample (459.6 eV), $L_{1.5}F_5T$-500, $L_{1.5}F_5T$-600 and $L_{1.5}F_5T$-700 show a slight deformation in the lower side of the binding energy, which corresponds to the formation of the Ti^{3+} species [48]. This behavior might be induced by fluorine substituting oxygen and lanthanum dopants. This is also supported by F_{1s} and La_{3d} XPS analysis. The existence of the Ti^{3+} species can inhibit the recombination of photogenerated electron–hole pairs [26,49].

The overall surface atomic content of F and Ti in $L_{1.5}F_5T$-500 were determined by XPS to be about 1.2 and 24.63%, respectively. Therefore, the overall surface atomic ratio of F to Ti in $L_{1.5}F_5T$-500 was about 4.86%. We can also see that the peak located at 688.4 eV is weak, which means that the substitutional fluorine ion content in the lattice of TiO_2 is smaller than that of physically adsorbed fluorine ions on the surface of TiO_2. The physically adsorbed fluorine ion content and the amount of fluorine ions in the crystal lattice on the surface of TiO_2 was calculated to be about 92.2 and 7.8%, respectively. This was calculated using the formula: $\delta_i = A_i/\sum A_i$, where A_i is the area of each peak. Similarly, the surface atomic ratios of La to Ti of $L_{1.5}F_5T$-500, $L_{1.5}F_5T$-600 and $L_{1.5}F_5T$-700 were also estimated from their corresponding XPS spectra to be about 1.97, 2.88 and 3.75%, respectively. It is clear that the La content in these samples is higher than the amount of nominal lanthanum and this is due to the formation of La_2O_3 on the surface of TiO_2. Additionally, the lanthanum content increases with calcination temperature, which means that La can easily move to the surface from the lattice of TiO_2 at higher calcination temperatures.

3.5. UV–vis absorption spectra

UV–vis diffuse reflection spectra of undoped TiO_2, L_0F_5T-500, $L_{1.5}F_0T$-500 and $L_{1.5}F_5T$-500 are shown in Fig. 5. These samples have a steep absorption edge located at ca. 389, 389, 396 and 393 nm, respectively, which can be attributed to the intrinsic absorption band derived from the bandgap transition. Compared with the three other samples, intraband gap states were observed for $L_{1.5}F_5T$-500 and these correspond to an absorption edge at about 440 nm. This behavior may be explained as follows: For the La-doped TiO_2 system, Ti^{4+} enters the lattice of lanthanum oxide during heat treatment, which creates a charge imbalance. The charge imbalance must be satiated and therefore Ti^{4+} is reduced to Ti^{3+}. Additionally, La and F doping also produce oxygen vacancies on the surface of TiO_2. A small amount of Ti^{3+} and oxygen vacancies extends the optical absorption of TiO_2 into the visible light region [50,51]. The presence of Ti^{3+} in $L_{1.5}F_5T$-500 was also indicated in the XPS spectrum. The intrinsic energy gap of undoped TiO_2, L_0F_5T-500, $L_{1.5}F_0T$-500 and $L_{1.5}F_5T$-500 as well as the intraband gap states of $L_{1.5}F_5T$-500 were roughly estimated to be about 3.18, 3.18, 3.13, 3.15 and 2.8 eV, which can be calculated from band-edge absorptions (λ_g) using the following equation.

$$E_g\,(\mathrm{eV}) = \frac{1240}{\lambda_g\,(\mathrm{nm})}$$

The absorption edge of L_0F_5T-500 and $L_{1.5}F_0T$-500 did not show a significant shift to the visible region, which means that single lanthanum or fluorine doping does not result in an absorption edge shift. This result can be explained by hybrid orbital theory. When TiO_2 is doped with fluorine, high density localized levels appear below the valence band of TiO_2, which is mainly composed of an F_{2p} state. This result has already been confirmed by theoretical band calculations [3]. On the other hand, lanthanum ions cannot enter the TiO_2 lattice, which means that lanthanum ions cannot decrease the bandgap of TiO_2 and thus cannot extend the optical absorption into the visible light region. However, Yu et al. [28] reported that their F-TiO_2 sample showed a weak red shift during absorption. Maeda et al. [18] also found that a $TiN_xO_yF_z$ sample showed a wide absorption band in the visible light region compared with a weak visible absorption of TiN_xO_y. These different results might be explained by considering the different synthesis methods used and the original materials, which might have resulted in different amounts of Ti^{3+} or oxygen vacancies and different high density localized levels below the valence band of TiO_2.

3.6. Photocatalytic activity

To investigate the effect of doping concentration and calcination temperature on photocatalytic activity, the decomposition of 4-CP with doped samples and bare TiO_2 under visible light and UV light irradiation were carried out.

Fig. 6A and B shows degradation rates versus illumination time and the total organic carbon (TOC) removal for 4-CP over undoped TiO_2, L_0F_5T-500, $L_{1.5}F_0T$-500, L_1F_5T-500, $L_{2.5}F_5T$-500, L_2F_5T-500 and $L_{1.5}F_5T$-500 after illumination under visible light for 4 h. The 4-CP degradation rates linearly increase at molar ratios of La to Ti from 0:100 to 1.5:100 and then decrease as the lanthanum content increases. Moreover, the degradation rate of 4-CP over $L_{1.5}F_5T$-500 can be estimated to be about 1.2 to 3.0 times higher than that of the other doped samples and undoped TiO_2, as shown in Fig. 6A. These results imply that the optimum molar ratio of La to Ti is 1.5:100. The TOC removal rate showed a similar trend to the degradation rate and 4-CP was mineralized efficiently with $L_{1.5}F_5T$-500 under visible light illumination. These results can be explained as follows: As the lanthanum content increases, the BET surface area increases (see Table 1) and 4-CP is effectively adsorbed by the sample, which results in higher photocatalytic activity. These results are consistent with the C/C_0 obtained from the adsorption–desorption equilibrium of 4-CP in the dark (see Table 2). La_2O_3 mounted on

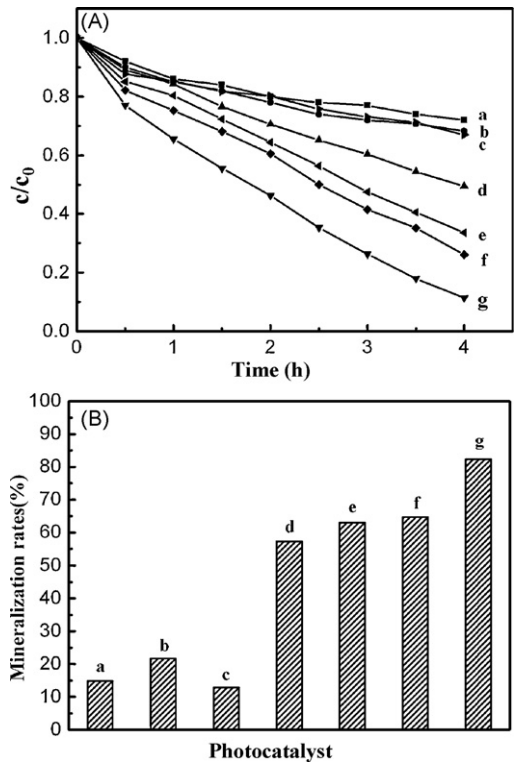

Fig. 6. The degradation rates (A) and total organic carbon (TOC) removal (B) of 4-chlorophenol photocatalyzed over (a) undoped TiO_2, (b) L_0F_5T-500, (c) $L_{1.5}F_0T$-500, (d) L_1F_5T-500, (e) $L_{2.5}F_5T$-500, (f) L_2F_5T-500, and (g) $L_{1.5}F_5T$-500.

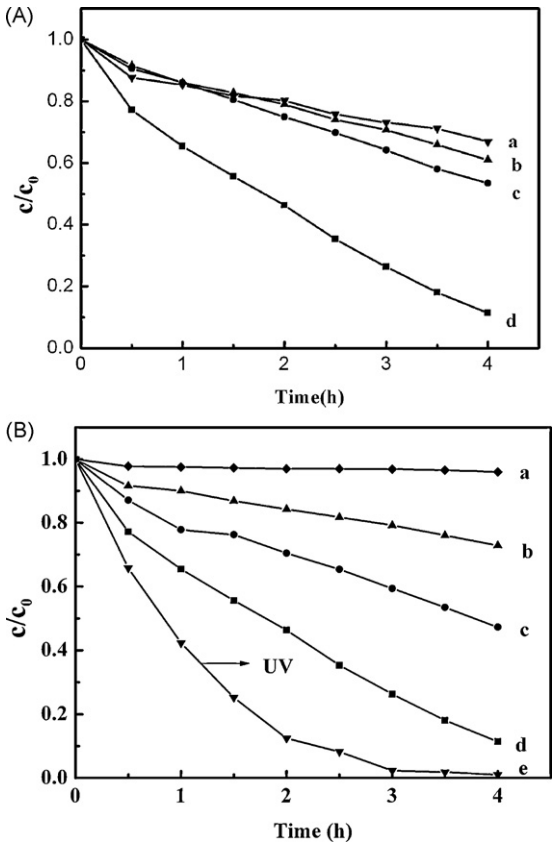

Fig. 7. The degradation rates of 4-chlorophenol photocatalyzed over (A): (a) $L_{1.5}F_0T$-500, (b) $L_{1.5}F_{20}T$-500, (c) $L_{1.5}F_{10}T$-500 and (d) $L_{1.5}F_5T$-500. (B): (a) without catalyst, (b) $L_{1.5}F_5T$-700, (c) $L_{1.5}F_5T$-600, (d) $L_{1.5}F_5T$-500 and (e) $L_{1.5}F_5T$-500 (UV irradiation).

the surface of TiO_2 can act as a barrier and thus inhibit the recombination of electron–hole pairs, which prolongs the lifetime of the electron–hole and thus enhances the quantum efficiency. However, when the concentration of lanthanum is increased continuously, the La_2O_3 coating on the surface of TiO_2 can inhibit the adsorption of 4-CP molecules on the surface of TiO_2 and thus decrease the number of 4-CP molecules adsorbed on the surface of TiO_2, which results in decreased photocatalytic activity.

The effect of fluorine doping content on the photocatalytic activity of $La_2O_3/TiO_{2-x}F_x$ is shown in Fig. 7A. The photocatalytic activity clearly increases substantially when the molar ratios of F to Ti changes from 0:100 to 5:100. The reason is that the acid active site on the surface of TiO_2 and suitable oxygen vacancies were created, while the oxidation potential of the photogenerated holes in the valence band of F-doped TiO_2 also increased. Further increasing the fluorine doping content, the photocatalytic activity started to decrease because of the formation of more oxygen vacancies and Ti^{3+} species, which can become the recombination center of photoinduced electrons and holes. This result means that the optimal molar ratio of F to Ti is 5:100.

Fig. 7B clearly shows that $L_{1.5}F_5T$-500 had a higher photocatalytic activity than $L_{1.5}F_5T$-600 and $L_{1.5}F_5T$-700. It is well known that the calcination temperature is an important factor for photocatalytic activity. When the calcination temperature is increased, it will facilitate the growth and agglomeration of fine grains and thus decrease the BET surface area, which results in a lower photocatalytic activity. On the other hand, it has been reported that the photocatalytic activity of rutile is lower than that of anatase [52]. In our case, when the calcination temperature was increased from 500 to 700 °C, the photocatalytic activities of $La_2O_3/TiO_{2-x}F_x$ decreased sharply because of the formation of a large quantity of rutile (see Fig. 1C).

$L_{1.5}F_5T$-500 exhibited the highest photocatalytic activity under UV light irradiation, as shown in Fig. 7B. This result can be explained as follows: The intrinsic bandgap is 3.2 eV, corresponding to UV radiation, for anatase TiO_2. Therefore, the electrons in the valence band will be easily excited to the 3d states of Ti^{3+} and/or oxygen vacancies and/or the conduction band under UV irradiation, leaving holes in the valence band. The photogenerated electrons combine with adsorbed oxygen to form superoxide anions and the holes react with OH^- to form hydroxyl radicals. The reactive oxygen species or hydroxyl radicals will react with 4-CP [34].

To investigate the self-degradation of 4-CP under visible light, a test without catalyst was carried out and this test showed that the degradation rate of 4-CP was only 4%, implying that 4-CP is stable under visible light irradiation [53].

In order to investigate the possibility of reuse for catalyst, $L_{1.5}F_5T$-500 was used to degrade 4-CP solutions four times. After the first run (visible light irradiation for 4 h), the suspension containing photocatalysts was centrifuged and the photocatalyst was washed three times with millipore water and dried at 100 °C for

Table 2
The data of C/C_0 of the adsorption–desorption equilibrium of 4-CP in dark.

	Sample							
	TiO_2-600	L_1F_5T-500	$L_{1.5}F_5T$-500	L_2F_5T-500	L_1F_5T-600	$L_{1.5}F_5T$-600	$L_{1.5}F_5T$-700	$L_{1.5}F_{10}T$-500
C/C_0	0.98	0.92	0.89	0.87	0.95	0.94	0.96	0.90

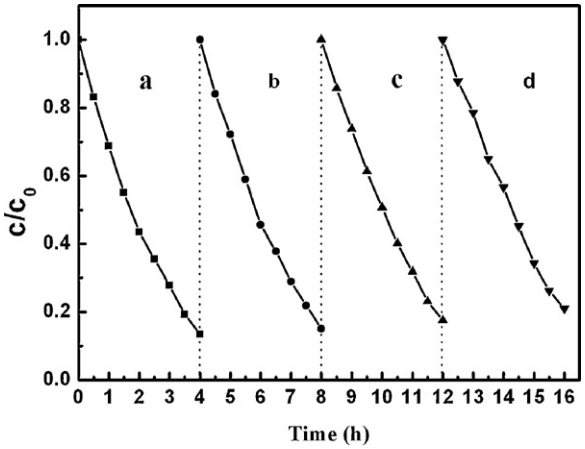

Fig. 8. The photocatalytic activity of (a) 1-cycle, (b) 2-cycle, (c) 3-cycle and (d) 4-cycle of $L_{1.5}F_5T$-500.

6 h. The recovered photocatalyst was subsequently used to degrade another fresh 4-CP solution (keep 4-CP concentration that is equal to the initial concentration of 4-CP as in the first circle) under the same irradiation conditions for 4 h. Then 3-cycle and 4-cycle were also carried out in the same process. The results are shown in Fig. 8. We found a relatively small decrease in photocatalytic activity after successive utilization cycles. The content of fluorine in the first supernatant was determined to be about 2×10^{-4} g L^{-1} using a chromatographic method. The surface of the recovered $L_{1.5}F_5T$-500 was studied by FTIR. Photocatalyst surface spectra (not shown) showed three bands (1631, 1398 and 1385 cm^{-1}) in the 1000–2000 cm^{-1} range. These bands are attributed to hydroxylated benzoic acids [54]. Therefore, the small decrease in the photocatalytic activity is due to the adsorption of the original compound and/or by-products on the active sites of the catalyst surface during repeated cycles.

3.7. Photocatalytic reaction mechanism

Recently, the reaction mechanism of the photocatalytic process has been widely investigated. Most researchers believe that the surface properties of TiO_2 such as the surface acidity, defects, oxygen vacancy, oxidation potential of holes and hydroxyl groups are important factors that determine the reaction efficiency [55–58]. The experimental results presented in this paper allow us to compile a schematic of the mechanism responsible for the interaction of $La_2O_3/TiO_{2-x}F_x$ with visible light.

(a) XPS investigations of La_{3d} reveal that La_2O_3 had formed and was located on the surface of TiO_2 and this inhibits the growth of crystal grains by restricting the coalescence of some smaller neighboring grains and thus enhances the TiO_2 surface area [36]. 4-CP can thus be effectively adsorbed by the sample, which results in higher photocatalytic activity. La_2O_3 mounted on the surface of TiO_2 can act as a space charge region and the electron–hole pairs within this region have been shown to be separated efficiently by an electric field before recombination [26], which can enhance the photocatalytic activity of TiO_2. However, if the doped La content is too high, the space charge region becomes very narrow and the depth of light penetration into TiO_2 greatly exceeds the space charge layer. In this case, recombination of the photoinduced electron–hole pairs becomes easier [26] and the photocatalytic activity begins to decrease. For the La-doped TiO_2 system, Ti^{4+} enters the lattice of La_2O_3 during heat treatment, which creates a charge imbalance. The charge imbalance must be satiated and, therefore, Ti^{4+} is reduced to Ti^{3+} [59]. The 3d states of Ti^{3+} below the conduction band can contribute to visible light absorption as the color center [34]. Therefore, the electrons in the valence band will be transferred to the 3d states of Ti^{3+} under visible light irradiation and the photogenerated electrons combine with O_2 adsorbed on the surface of TiO_2 to form superoxide anions. The reactive oxygen species will react with 4-CP [34]. After a series of reactions, 4-CP molecules are finally degraded into CO_2 and H_2O.

(b) XPS spectra of F_{1s} showed that the possible formation of fluorine should be taken into account for both the surface and bulk F^- dopants as these are important factors for photocatalysis. First, surface fluorine can increase the surface acidity because of the strong electronegativity of fluorine and this can effectively improve the adsorption of the reacting organic molecules. Second, three positive roles of bulk F^- dopants in photocatalysis are: (1) The doped fluorine ion in the O^{2-} sites of the TiO_2 lattice needs one extra electron for charge compensation. This electron localizes on a lattice cation causing its reduction from Ti^{4+} to Ti^{3+}. The effect of Ti^{3+} on visible light photocatalysis has been discussed above. (2) Oxygen vacancies created by fluorine doping below the conduction band are responsible for visible light absorption of TiO_2 and directly provide the active species for the photocatalytic reaction [33]. (3) Doped fluorine can result in a localized level with high density and this is present below the valence band of TiO_2, which mainly consists of the F_{2p} state [18,35]. Therefore, the holes in the valance band are trapped at these localized levels and are less mobile, which is beneficial in increasing the oxidation potential of the valance band holes and capturing the surface hydroxyls to produce •OH [60], as shown in Scheme 1. •OH is a powerful oxidant during the degradation of 4-CP.

In summary, the synergetic effect of lanthanum and fluorine effectively tunes the energy band structure, improves the surface area and enhances the visible light photocatalytic activity of TiO_2.

4. Conclusions

We found that $La_2O_3/TiO_{2-x}F_x$ shows an extended optical absorption range and also has higher visible light photocatalytic activity compared with undoped TiO_2. In particular, the visible light photocatalytic activity of $L_{1.5}F_5T$-500 was 1.2–3.0 times more than that of other samples tested. We believe that lanthanum increases the surface area and decreases recombination of the photoinduced electron–hole pairs. When fluorine atoms are incorporated into TiO_2 or loaded onto the surface of TiO_2, the oxidation potential of the photogenerated holes in the valence band and the active sites on the surface of TiO_2 are much improved. In summary, this work has demonstrated that extending the spectral response into the visible light region and enhancing the photocatalytic activity can be achieved by tuning the energy band structure and improving the surface area of TiO_2 by the synergetic effect of fluorine and lanthanum.

Acknowledgments

We gratefully acknowledge the financial supports by Shanghai Municipal Education Commission (No. 07SG37), Natural Science Foundation of China (No. 50772022), National Key Technology R&D Program (No. 2006BAA04B02-01), Shanghai Leading Academic Discipline Project (B603), the Cultivation Fund of the Key Scientific and Technical Innovation Project (No. 708039), and the Program of Introducing Talents of Discipline to Universities (No. 111-2-04).

References

[1] T. Morikawa, T. Ohwaki, K. Suzuki, S. Moribe, S. Tero-Kubota, Visible-light-induced photocatalytic oxidation of carboxylic acids and aldehydes over N-doped TiO_2 loaded with Fe, Cu or Pt, Appl. Catal. B: Environ. 83 (2008) 56–62.

[2] K.L. Lv, H.S. Zuo, J. Sun, K.J. Deng, S.C. Liu, X.F. Li, D.Y. Wang, (Bi, C and N) codoped TiO_2 nanoparticles, J. Hazard. Mater. 161 (2009) 396–401.

[3] R. Asahi, T. Morikawa, T. Ohwaki, K. Aoki, Y. Taga, Visible-light photocatalysis in nitrogen-doped titanium oxides, Science 293 (2001) 269–271.

[4] S.U.M. Khan, M. Al-Shahry, W.B. Ingler Jr., Efficient photochemical water splitting by a chemically modified n-TiO_2, Science 297 (2002) 2243–2245.

[5] S.X. Liu, X.Y. Chen, A visible light response TiO_2 photocatalyst realized by cationic S-doping and its application for phenol degradation, J. Hazard. Mater. 152 (2008) 48–55.

[6] M.A. Fox, M.T. Dulay, Heterogeneous photocatalysis, Chem. Rev. 93 (1993) 341–357.

[7] H. Ozaki, N. Fujimoto, S. Iwamoto, M. Inoue, Photocatalytic activities of NH_3-treated titanias modified with other elements, Appl. Catal. B: Environ. 70 (2007) 431–436.

[8] W.K. Jo, J.T. Kim, Application of visible-light photocatalysis with nitrogen-doped or unmodified titanium dioxide for control of indoor-level volatile organic compounds, J. Hazard. Mater. 164 (2009) 360–366.

[9] X.Z. Shen, Z.C. Liu, S.M. Xie, J. Guo, Degradation of nitrobenzene using titania photocatalyst co-doped with nitrogen and cerium under visible light illumination, J. Hazard. Mater. 162 (2009) 1193–1198.

[10] Q.H. Zhang, W.G. Fan, L. Gao, Anatase TiO_2 nanoparticles immobilized on ZnO tetrapods as a highly efficient and easily recyclable photocatalyst, Appl. Catal. B: Environ. 76 (2007) 168–173.

[11] H. Einaga, M. Harada, S. Futamura, T. Ibusuki, Generation of active sites for CO photooxidation on TiO_2 by platinum deposition, J. Phys. Chem. B 107 (2003) 9290–9297.

[12] T.Z. Tong, J.L. Zhang, B.Z. Tian, F. Chen, D.N. He, Preparation of Fe^{3+}-doped TiO_2 catalysts by controlled hydrolysis of titanium alkoxide and study on their photocatalytic activity for methyl orange degradation, J. Hazard. Mater. 155 (2008) 572–579.

[13] Z.M. El-Bahy, A.A. Ismail, R.M. Mohamed, Enhancement of titania by doping rare earth for photodegradation of organic dye (Direct Blue), J. Hazard. Mater. 166 (2009) 138–143.

[14] Z.J. Li, W.Z. Shen, W.S. He, X.T. Zu, Effect of Fe-doped TiO_2 nanoparticle derived from modified hydrothermal process on the photocatalytic degradation performance on methylene blue, J. Hazard. Mater. 155 (2008) 590–594.

[15] M. Jin, Y. Nagaoka, K. Nishi, K. Ogawa, S. Nagahata, T. Horikawa, M. Katoh, T. Tomida, J. Hayashi, Adsorption properties and photocatalytic activity of TiO_2 and La-doped TiO_2, Adsorption 14 (2008) 257–263.

[16] C. Burda, Y. Lou, X. Chen, A.C. Samina, J. Stout, J.L. Gole, Enhanced nitrogen doping in TiO_2 nanoparticles, Nano. Lett. 3 (2008) 1049–1051.

[17] H. Irie, Y. Watanabe, K. Hashimoto, Nitrogen-concentration dependence on photocatalytic activity of $TiO_{2-x}N_x$ powders, J. Phys. Chem. B 107 (2003) 5483–5486.

[18] K. Maeda, Y. Shimodaira, B. Lee, K. Tentaro, D. Lu, H. Kobayashi, K. Domen, Studies on $TiN_xO_yF_z$ as a visible-light-responsive photocatalyst, J. Phys. Chem. C 111 (2007) 18264–18270.

[19] D. Li, H.J. Haneda, S. Hishita, N.K. Ohashi, Visible-light-driven N–F-codoped TiO_2 photocatalysts. 1. Synthesis by spray pyrolysis and surface characterization, Chem. Mater. 17 (2005) 2588–2595.

[20] X.B. Chen, C. Burda, The electronic origin of the visible-light absorption properties of C-, N- and S-doped TiO_2 nanomaterials, J. Am. Chem. Soc. 130 (2008) 5018–5019.

[21] D.M. Chen, D. Yang, Q. Wang, Z.Y. Jang, Effects of boron doping on photocatalytic activity and microstructure of titanium dioxide nanoparticles, Ind. Eng. Chem. Res. 45 (2006) 4110–4116.

[22] W. Zhao, W.H. Ma, C.C. Chen, J.C. Zhao, Z.G. Shuai, Efficient degradation of toxic organic pollutants with $Ni_2O_3/TiO_{2-x}B_x$ under visible light irradiation, J. Am. Chem. Soc. 126 (2004) 4782–4783.

[23] S. In, A. Orlov, R. Berg, F. Garcia, S. Pedrosa-Jimenez, M.S. Tikhov, D.S. Wright, R.M. Lambert, Effective visible light-activated B-doped and B, N-codoped TiO_2 photocatalysts, J. Am. Chem. Soc. 129 (2007) 13790–13791.

[24] Y.N. Huo, X.Y. Zhang, Y. Jin, J. Zhu, H.X. Li, Highly active $La_2O_3/Ti_{1-x}B_xO_2$ visible light photocatalysts prepared under supercritical conditions, Appl. Catal. B: Environ. 83 (2008) 78–84.

[25] S. Yin, K. Ihara, Y. Aita, M. Komatsu, T. Sato, Visible-light induced photocatalytic activity of $TiO_{2-x}A_y$ (A = N, S) prepared by precipitation route, J. Photochem. Photobiol. A 179 (2006) 105–114.

[26] Z.Q. He, X. Xu, S. Song, L. Xie, J.J. Tu, J.M. Chen, B. Yan, A visible light-driven titanium dioxide photocatalyst codoped with lanthanum and iodine: an application in the degradation of oxalic acid, J. Phys. Chem. C 112 (2008) 16431–16437.

[27] W.K. Ho, J.C. Yu, S.C. Lee, Synthesis of hierarchical nanoporous F-doped TiO_2 spheres with visible light photocatalytic activity, Chem. Commun. (2006) 1115–1117.

[28] J.C. Yu, J.G. Yu, W.K. Ho, Z.T. Jiang, L.Z. Zhang, Effects of F-doping on the photocatalytic activity and microstructures of nanocrystalline TiO_2 powders, Chem. Mater. 14 (2002) 3808–3816.

[29] X.X. Yang, C.D. Cao, L. Ericksona, K. Hohn, R. Maghirang, K. Klabunde, Synthesis of visible-light-active TiO_2-based photocatalysts by carbon and nitrogen doping, J. Catal. 260 (2008) 128–133.

[30] D.M. Chen, Z.Y. Jiang, J.Q. Geng, Q. Wang, D. Yang, Carbon and nitrogen co-doped TiO_2 with enhanced visible-light photocatalytic activity, Ind. Eng. Chem. Res. 46 (2007) 2741–2746.

[31] H.Q. Sun, Y. Bai, Y.P. Cheng, W.Q. Jin, N.P. Xu, Preparation and characterization of visible-light-driven carbon–sulfur-codoped TiO_2 photocatalysts, Ind. Eng. Chem. Res. 45 (2006) 4971–4976.

[32] V. Gombac, L. De Rogatis, A. Gasparotto, G. Vicario, T. Montini, D. Barreca, G. Balducci, P. Fornasiero, E. Tondello, M. Graziani, TiO_2 nanopowders doped with boron and nitrogen for photocatalytic applications, Chem. Phys. 339 (2007) 111–123.

[33] D. Li, H. Haneda, S. Hishita, N. Ohashi, N.K. Labhsetwar, Fluorine-doped TiO_2 powders prepared by spray pyrolysis and their improved photocatalytic activity for decomposition of gas-phase acetaldehyde, J. Fluorine Chem. 126 (2005) 69–77.

[34] J. Wang, D.N. Tafen, J.P. Lewis, Z.L. Hong, A. Manivannan, M.J. Zhi, M. Li, N.Q. Wu, Origin of photocatalytic activity of nitrogen-doped TiO_2 nanobelts, J. Am. Chem. Soc. 131 (2009) 12290–12297.

[35] C.D. Valentin, E. Finazzi, G. Pacchioni, Density functional theory and electron paramagnetic resonance study on the effect of N–F codoping of TiO_2, Chem. Mater. 20 (2008) 3706–3714.

[36] K.T. Ranjit, H. Cohen, I. Willner, S. Bossmann, A.M. Braun, Lanthanide oxide-doped titanium dioxide: effective photocatalysts for the degradation of organic pollutants, J. Mater. Sci. 34 (1999) 5273–5280.

[37] F.B. Li, X.Z. Li, M.F. Hou, Photocatalytic degradation of 2-mercaptobenzothiazole in aqueous La^{3+}–TiO_2 suspension for odor control, Appl. Catal. B: Environ. 48 (2004) 185–194.

[38] X.Z. Ding, X.H. Liu, Correlation between anatase-to-rutile transformation and grain growth in nanocrystalline titania powders, J. Mater. Res. 13 (1998) 2556–2559.

[39] B.M. Reddy, I. Ganesh, Characterization of La_2O_3-TiO_2 and V_2O_5/La_2O_3-TiO_2 catalysts and their activity for synthesis of 2,6-dimethylphenol, J. Mol. Catal. A: Chem. 169 (2001) 207–223.

[40] S.C. Padmanabhan, S.C. Pillai, J. Colreavy, S. Balakrishnan, D.E. McCormack, T.S. Perova, Y. Gunko, S.J. Hinder, J.M. Kelly, A simple sol-gel processing for the development of high-temperature stable photoactive anatase titania, Chem. Mater. 19 (2007) 4474–4481.

[41] Y. Matsumoto, M. Murakami, T. Shono, T. Hasegawa, T. Fukumura, M. Kawasaki, P. Ahmet, T. Chikyow, S. Koshihara, H. Koinuma, Room-temperature ferromagnetism in transparent transition metal-doped titanium dioxide, Science 291 (2001) 854–856.

[42] K.S.W. Sing, D.H. Everett, R.A.W. Haul, L. Moscou, R.A. Pierotti, J. Rouquerol, T. Sieminewska, Reporting physisorption data for gas/solid systems with special reference to the determination of surface area and porosity, Pure Appl. Chem. 57 (1985) 603–619.

[43] W.J. Ren, Z.H. Ai, F.L. Jia, L.Z. Zhang, X.X. Fan, Z.G. Zou, Low temperature preparation and visible light photocatalytic activity of mesoporous carbon-doped crystalline TiO_2, Appl. Catal. B: Environ. 69 (2007) 138–144.

[44] S. Shanmugam, A. Gabashvili, D.S. Jacob, J.C. Yu, A. Gedanken, Synthesis and characterization of TiO_2@C core–shell composite nanoparticles and evaluation of their photocatalytic activities, Chem. Mater. 18 (2006) 2275–2282.

[45] L.Z. Zhang, J.C. Yu, A sonochemical approach to hierarchical porous titania spheres with enhanced photocatalytic activity, Chem. Commun. (2003) 2078–2079.

[46] I.G. Austin, N.F. Mott, Polarons in crystalline and non-crystalline materials, Adv. Phys. 50 (2001) 757–812.

[47] A.M. Czoska, S. Livraghi, M. Chiesa, E. Giamello, S. Agnoli, G. Granozzi, E. Finazzi, C.D. Valentin, G. Pacchioni, The nature of defects in fluorine-doped TiO_2, J. Phys. Chem. C 112 (2008) 8951–8956.

[48] Q. Xiao, J. Zhang, C. Xiao, Z.C. Si, X.K. Tan, Solar photocatalytic degradation of methylene blue in carbon-doped TiO_2 nanoparticles suspension, Solar Energy 82 (2008) 706–713.

[49] X.T. Hong, Z.P. Wang, W.M. Cai, F. Lu, J. Zhang, Y.Z. Yang, N. Ma, Y.J. Liu, Visible-light-activated nanoparticle photocatalyst of iodine-doped titanium dioxide, Chem. Mater. 17 (2005) 1548–1552.

[50] K. Nukumizu, J. Nunoshige, T. Takata, J.N. Kondo, M. Hara, H. Kobayashi, K. Domen, $TiN_xO_yF_z$ as a stable photocatalyst for water oxidation in visible light ($\lambda < 570$ nm), Chem. Lett. 32 (2003) 196–197.

[51] E.A. Reyes-Garcia, Y.P. Sun, D. Raftery, Solid-state characterization of the nuclear and electronic environments in a boron-fluoride co-doped TiO_2 visible-light photocatalyst, J. Phys. Chem. C 111 (2007) 17146–17154.

[52] X.J. Quan, H.Q. Tan, Q.H. Zhao, X.M. Sang, Preparation of lanthanum-doped TiO_2 photocatalysts by coprecipitation, J. Mater. Sci. 42 (2007) 6287–6296.

[53] T. Lindgren, J.M. Mwabora, E. Avendan, J. Jonsson, A. Hoel, C.G. Granqvist, S.E. Lindquist, Photoelectrochemical and optical properties of nitrogen doped titanium dioxide films prepared by reactive DC magnetron sputtering, J. Phys. Chem. B 107 (2003) 5709–5716.

[54] J. Araña, E.T. Rendón, J.M.D. Rodriguez, J.A.H. Melián, O.G. Diaz, J.P. Peña, High concentrated phenol and 1,2-propylene glycol water solutions treatment by photocatalysis catalyst recovery and re-use, Appl. Catal. B: Environ. 30 (2001) 1–10.

[55] J.W. Tang, H.D. Quan, J.H. Ye, Photocatalytic properties and photoinduced hydrophilicity of surface-fluorinated TiO_2, Chem. Mater. 19 (2007) 116–122.

[56] Y. Huang, W.K. Ho, S.C. Lee, L.Z. Zhang, G.S. Li, J.C. Yu, Effect of carbon doping on the mesoporous structure of nanocrystalline titanium dioxide and

its solar-light-driven photocatalytic degradation of NO_x, Langmuir 24 (2008) 3510–3516.
[57] Y.T. Kwon, K.Y. Song, W.I. Lee, G.J. Choi, Y.R. Do, Photocatalytic behavior of WO_3-loaded TiO_2 in an oxidation reaction, J. Catal. 191 (2000) 192–199.
[58] V. Keller, P. Bernhardt, F. Grain, Photocatalytic oxidation of butyl acetate in vapor phase on TiO_2, Pt/TiO_2 and WO_3/TiO_2 catalysts, J. Catal. 215 (2003) 129–138.
[59] M. Miyauchi, M. Takashio, H. Tobimatsu, Photocatalytic activity of $SrTiO_3$ codoped with nitrogen and lanthanum under visible light illumination, Langmuir 20 (2004) 232–236.
[60] T. Tachikawa, S. Tojo, K. Kawai, M. Endo, M. Fujitsuka, T. Ohno, K. Nishijima, Z. Miyamoto, T. Majima, Photocatalytic oxidation reactivity of holes in the sulfur- and carbon-doped TiO_2 powders studied by time-resolved diffuse reflectance spectroscopy, J. Phys. Chem. B 108 (2004) 19299–19306.